nature chemical biology

ARTICLE

PUBLISHED ONLINE: 12 MAY 2013 | DOI: 10.1038/NCHEMBIO.1252

Chemically inducible diffusion trap at cilia reveals molecular sieve–like barrier

Yu-Chun Lin[1], Pawel Niewiadomski[2,3,7], Benjamin Lin[1,4,7], Hideki Nakamura[5,7], Siew Cheng Phua[1], John Jiao[1], Andre Levchenko[4], Takafumi Inoue[5], Rajat Rohatgi[3] & Takanari Inoue[1,6]*

Primary cilia function as specialized compartments for signal transduction. The stereotyped structure and signaling function of cilia inextricably depend on the selective segregation of molecules in cilia. However, the fundamental principles governing the access of soluble proteins to primary cilia remain unresolved. We developed a methodology termed 'chemically inducible diffusion trap at cilia' to visualize the diffusion process of a series of fluorescent proteins ranging in size from 3.2 nm to 7.9 nm into primary cilia. We found that the interior of the cilium was accessible to proteins as large as 7.9 nm. The kinetics of ciliary accumulation of this panel of proteins was exponentially limited by their Stokes radii. Quantitative modeling suggests that the diffusion barrier operates as a molecular sieve at the base of cilia. Our study presents a set of powerful, generally applicable tools for the quantitative monitoring of ciliary protein diffusion under both physiological and pathological conditions.

A primary cilium is an antenna-like organelle protruding from the apical surface of most cells in a wide variety of organisms[1]. Primary cilia regulate several signaling systems such as phototransduction, olfaction and developmental pathways[2]. To achieve these functions, primary cilia accumulate a specific set of biomolecules, including membrane receptors and their downstream soluble effectors. As biosynthetic machinery is not present in primary cilia[3], these biomolecules must be transported into primary cilia from the cell body. Thus, understanding protein transport across the physical separation between the site of protein synthesis (the cell body) and the site of protein function (the cilium) is of fundamental importance in the field of ciliary biology and cilia-based diseases[4].

The trafficking of membrane proteins into primary cilia has been intensively studied[5–7]. At the ciliary neck, there is a diffusion barrier regulated by Septin2 and other proteins that limit free lateral diffusion of membrane proteins from the contiguous plasma membrane[5,7]. This defining feature maintains a distinct composition of lipids and membrane proteins inside primary cilia[4]. Although the soluble environment in the ciliary lumen is specialized as well, the mechanisms that regulate the transport of soluble molecules into or out of primary cilia remain poorly understood.

The transport of soluble molecules between the cytosol and the ciliary lumen has been most rigorously examined in rod photoreceptor cells, which have a connecting cilium that provides a conduit between the cell body and the outer segment[8]. The massive vectorial transport of arrestin, a soluble protein, across the connecting cilium into the outer segment was shown to occur by simple diffusion driven by a concentration gradient generated when photons expose arrestin-binding sites on rhodopsin, which is highly concentrated in the outer segment[9]. In this system, monomers, dimers and trimers of GFP freely diffuse across the connecting cilium, suggesting that there is no fixed pore that limits the diffusion of soluble proteins of at least up to 80 kDa[10].

In contrast to these studies of photoreceptor cilia, a recent study proposed that molecules above 67 kDa are excluded from primary cilia in epithelial cells by a fixed pore at the ciliary base that has similar properties and molecular composition to the nuclear pore complex (NPC)[11]. In this study, the kinetics of accumulation in cilia was not directly monitored; instead, the ratio of fluorescence between the cilium and the cytosol at a given time point after microinjection of a labeled tracer was measured. Because diffusion is a kinetic process, such end-point assays cannot distinguish between differences in the rate of diffusion and differences in the propensity of molecules to occupy the cytoplasm and the cilium. A notable example of this is found in dark-adapted photoreceptors, where arrestin is excluded from the outer segment because of molecular crowding effects and not because its diffusion is restricted across the connecting cilium[10].

These considerations and the divergent conclusions reached by studies in rods and cultured cells prompted us to use chemically inducible dimerization to visualize ciliary diffusion in living cells. Our technique bypasses the need for perturbations such as microinjection or detergent permeabilization, which are commonly used to introduce diffusion probes into cells. With both high sensitivity and fine temporal resolution, we explored the ciliary diffusion barrier faced by soluble cytoplasmic proteins ranging in Stokes radius (R_s) from 3.2 nm to 7.9 nm (molecular weight 40–650 kDa). Although the rate of ciliary influx of this series of probes was strongly dependent on their size, the ciliary diffusion barrier allowed the entry of soluble proteins with an R_s as large as 7.9 nm. Our kinetic data, obtained using a large series of diffusion probes, were most consistent with a sieve-like barrier at cilia whose mesh radius is larger than 7.9 nm. The present study highlights a powerful technique that enables quantitative characterization of the ciliary diffusion barrier for soluble proteins and substantially revises our physical model of this barrier.

RESULTS

Trapping soluble proteins inside cilia of live cells

The measurement of diffusion between two compartments requires the presence of a concentration gradient. We begin by describing

[1]Department of Cell Biology, Center for Cell Dynamics, School of Medicine, Johns Hopkins University, Baltimore, Maryland, USA. [2]Department of Medicine, School of Medicine, Stanford University, Stanford, California, USA. [3]Department of Biochemistry, School of Medicine, Stanford University, Stanford, California, USA. [4]Department of Biomedical Engineering, Johns Hopkins University, Baltimore, Maryland, USA. [5]Department of Life Science and Medical Bioscience, School of Advanced Science and Engineering, Waseda University, Tokyo, Japan. [6]PRESTO, Japan Science and Technology Agency, Saitama, Japan. [7]These authors contributed equally to the work. *e-mail: jctinoue@jhmi.edu

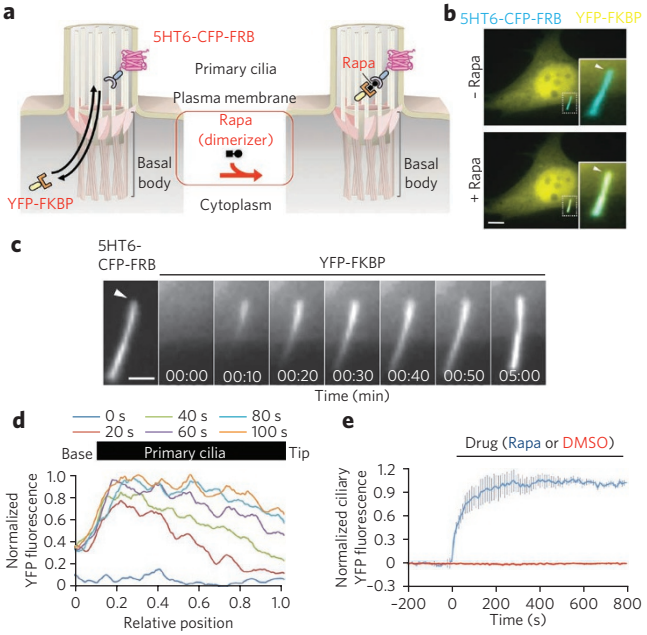

Figure 1 | Chemically inducible diffusion trap of soluble proteins inside primary cilia. (**a**) Schematic diagram of ciliary influx of cytosolic YFP-FKBP proteins using a chemically induced dimerization system. Available cytosolic YFP-FKBP in primary cilia can be trapped by rapamycin (Rapa) to a primary cilia membrane marker, 5HT6-CFP-FRB. (**b**) Fluorescence image of NIH3T3 cells expressing 5HT6-CFP-FRB (cyan) and YFP-FKBP (yellow) before and 5 min after addition of 100 nM rapamycin, which induced accumulation of YFP-FKBP in the 5HT6-CFP-FRB–labeled primary cilia. Insets (enlarged views of the boxed regions) show cilia visualized as overlays of the color channels. Scale bars, 10 µm. (**c**) Video frames illustrating the translocation of YFP-FKBP into 5HT6-CFP-FRB–labeled primary cilia before and after addition of 100 nM rapamycin. The arrowhead indicates the base of the cilia. Scale bars, 3 µm. (**d**) A line-scan analysis of the YFP signal intensity along the primary cilia after addition of 100 nM rapamycin for the indicated time. The cilium is indicated horizontally, with its tip on the right (n = 3 cells from three independent experiments). (**e**) Time course of YFP fluorescence intensity in primary cilia of the cells treated with 100 nM rapamycin (blue) or 0.1% DMSO (red). Error bars represent s.e.m. (n = 16 cells from three independent experiments).

a new technique for generating such a gradient between the cytoplasm and the cilium by using a high-affinity interaction to trap soluble proteins that diffuse into primary cilia. The gradient in this approach is conceptually identical to the arrestin gradient generated across the photoreceptor connecting cilium when light generates arrestin-binding sites on rhodopsin in the outer segment[8]. The basis of our technology is chemically inducible dimerization[12], where a chemical dimerizer such as rapamycin induces the dimerization of FK506 binding protein (FKBP) and FKBP-rapamycin binding domain (FRB) (**Fig. 1a**). By localizing the FRB partner protein in cilia, we hypothesized that rapamycin addition could be used to trap any FKBP fusion protein that diffused into cilia, thus generating a sink that would set up a concentration gradient of the FKBP fusion protein across the putative ciliary diffusion barrier.

We used 5-hydroxytryptamine receptor 6 (5HT6)[13] to target a fusion protein of CFP and FRB to the ciliary membrane (**Fig. 1a**). Immunofluorescence images confirmed that the resulting fusion protein, 5HT6-CFP-FRB, was highly enriched in primary cilia (**Supplementary Results**, **Supplementary Fig. 1**). When we transfected NIH3T3 cells together with 5HT6-CFP-FRB and YFP-tagged FKBP (YFP-FKBP), the former was highly enriched in cilia, and the latter was distributed throughout the cytoplasm (**Fig. 1b**). Addition of rapamycin for 5 min led to a marked increase in YFP fluorescence in primary cilia (**Fig. 1b**). Time-lapse, dual-color fluorescence imaging revealed the spatial dynamics and kinetics of the process (**Supplementary Video 1**). More specifically, a time series of YFP fluorescence in primary cilia and line scan analysis demonstrated that YFP-FKBP gradually accumulated in cilia from the base to the tip until saturation was reached, presumably because all of the 5HT6-CFP-FRB binding sites were occupied, and thus the concentration gradient was abolished (**Fig. 1c,d**). Lateral diffusion of YFP-FKBP, 5HT6-CFP-FRB and rapamycin complexes within the cilia membrane could also contribute to the spatial temporal evolution of the YFP fluorescence profiles. The time required for half-maximal accumulation in cilia ($t_{1/2}$) for YFP-FKBP was 57 ± 5 s (**Fig. 1e**). To rule out the possibility that our results were cell type–specific, we tested the influx assay in another cell type, IMCD3, commonly used as a model in cilia biology. No significant difference was found in the influx rate of YFP-FKBP into primary cilia between NIH3T3 and IMCD3 cells (P = 0.749, 57 ± 5 s and 68 ± 32 s, respectively; **Supplementary Fig. 2**).

Several control experiments were performed to establish that YFP-FKBP accumulation was caused by the trapping of YFP-FKBP that diffused into cilia. During the experimental time period, we did not observe an increase in the amount of 5HT6-CFP-FRB bait in primary cilia (**Supplementary Fig. 3**). Second, trapping required a freely diffusing form of YFP-FKBP because a variant of YFP-FKBP anchored to the cytoplasmic face of the endoplasmic reticulum (YFP-FKBP-Cb5) by a single transmembrane domain could not be recruited to cilia by rapamycin[14] (**Supplementary Fig. 4**). Finally, we sought to exclude the possibility that the observed accumulation of YFP-FKBP was not due to trapping within cilia but rather due to the transport of complexes between 5HT6-CFP-FRB, YFP-FKBP and rapamycin that formed outside cilia. Previous reports have shown that the diffusion of 5HT6 across the ciliary membrane protein barrier is slow (hours)[7] compared to our assay timescale (minutes). We confirmed the kinetics of 5HT6 by performing a fluorescence recovery after photobleaching (FRAP) assay. 5HT6-GFP and 5HT6-GFP-FRB fluorescence did not recover inside primary cilia for 90 min after photobleaching (**Supplementary Fig. 5**), suggesting that there was negligible flux of new 5HT6-GFP-FRB molecules into the cilium during our experiments.

Taken together, these studies indicate that the addition of rapamycin produces a diffusion trap in primary cilia, acutely generating a concentration gradient that can be used to follow the diffusion of any protein fused to YFP-FKBP.

Orthogonal dimerizer systems for ciliary trapping

We also constructed a ciliary diffusion trap using an orthogonal chemical dimerizer system that uses a gibberellin analog (GA_3-AM) and two completely different protein domains[15] instead of FRB and FKBP. Upon addition of GA_3-AM, YFP-labeled GIBBERELLIN INSENSITIVE DWARF1 (YFP-GID1) accumulated in primary cilia carrying 5HT6 fused to the N-terminal 92 residues of Gibberellin insensitive (5HT6-GAI(S)) (**Supplementary Fig. 6**). The influx rate of YFP-GID1 into primary cilia was roughly three times slower than that of YFP-FKBP (185 ± 29 s versus 57 ± 4.6 s). This difference could be due to the larger size of YFP-GID1 (616 residues) compared to YFP-FKBP (392 residues), differences in the permeability of the chemical dimerizers or dimerization affinity. These results suggest that the FKBP-FRB and GID1-GAI(S) systems can be used together in cells to induce two separate dimerization-driven signaling manipulations.

Probing the diffusion barrier of primary cilia

We performed ciliary trapping experiments using YFP-FKBP proteins that were fused to a series of diffusion probe proteins whose native molecular weights ranged from 40 kDa to 650 kDa (**Table 1**).

Table 1 | Size and influx rate of FKBP probe proteins

Test proteins	Experimental R_s (nm)[a]	Experimental MW (kDa)[b]	Estimated MW (kDa)[c]	$t_{1/2}$ accumulation time (s)	Slope of integrated fluorescence in cilia (AU)[d]	Diffusion coefficients inside cilia ($\mu m^2 s^{-1}$)
YFP-FKBP	3.2	40	43	57 ± 5	130 ± 25	5.58 ± 0.52
YFP-FKBP-PKIM	4.1	39	49	60 ± 2	248 ± 65	5.33 ± 1.5
YFP-FKBP-Grp1(229–772)	4.1	57	62	101 ± 33	69 ± 11	3.99 ± 0.54
YFP-FKBP-Grp1(229–1200)	4.4	72	78	95 ± 21	100 ± 29	2.57 ± 0.61
YFP-luciferase-FKBP	4.4	100	101	229 ± 101	119 ± 17	1.44 ± 0.19
YFP-FKBP-luciferase	4.5	100	102	197 ± 83	30 ± 7	0.91 ± 0.23
YFP-FKBP-Grp1(1–772)	4.9	69	71	130 ± 22	134 ± 85	1.97 ± 0.74
YFP-FKBP-Grp1(1–1200)	5.0	88	87	266 ± 59	52 ± 13	0.69 ± 0.37
YFP-FKBP-Tiam1	5.1	124	107	193 ± 64	29 ± 9	0.90 ± 0.25
YFP-FKBP-ΔN β-Gal	6.3	322	305	466 ± 83	45 ± 27	0.69 ± 0.26
YFP-FKBP-β-Gal	7.6	659	622	813 ± 171	18 ± 13	0.32 ± 0.15
YFP-β-Gal-FKBP	7.9	651	626	997 ± 334	14 ± 5	0.28 ± 0.25

[a]Measured and calculated from a native gel filtration assay with internal standards. [b]Calculated from a western blot analysis. [c]Estimated on the basis of amino acid sequences. [d]Corresponds to *J* in equation (1). AU, arbitrary units.

These test proteins were chosen according to the following criteria: (i) uniform distribution in the cytosol (**Supplementary Fig. 7**), (ii) lack of effect on the localization of 5HT6-CFP-FRB (**Supplementary Fig. 7**) and (iii) lack of effect on the length of cilia (**Supplementary Fig. 8**). To determine the R_s of these proteins, we fractionated extracts made from cells overexpressing each YFP-tagged protein by gel filtration chromatography and calculated the R_s of each protein using a set of standards (**Supplementary Fig. 9**). The YFP-FKBP fusion proteins varied in size between 32 Å and 79 Å (**Table 1**). Of note, YFP-FKBP fusion proteins of full-length β-galactosidase (YFP-FKBP–β-Gal) and its N-terminally truncated variant (YFP-FKBP–ΔN β-Gal) formed a tetramer (R_s: 79 Å) and dimer (R_s: 62 Å), respectively, as described previously[16,17]. We measured the rate at which these proteins accumulated in primary cilia after the addition of rapamycin. Our results indicated a decrease in accumulation rates as protein size increased (**Fig. 2a** and **Supplementary Fig. 7**). A single exponential curve fit the data (R^2 = 0.85), suggesting the existence of a diffusion barrier that is dependent on protein size (**Fig. 2a**). **Figure 2b** illustrates representative fluorescence images of the ciliary accumulation of three proteins (YFP-FKBP, YFP-FKBP-luciferase and YFP-FKBP–β-Gal) after rapamycin addition.

One concern in the above experiment was that we were detecting the translocation of smaller degradation products of the probe proteins and not the full-length proteins. To address this possibility, we constructed two additional fusion proteins, YFP-luciferase-FKBP and YFP–β-Gal–FKBP, in which the YFP used for detection by fluorescence microscopy was separated from the FKBP used for dimerization by the probe protein. In this arrangement, any degradation product would separate the YFP from the FKBP, rendering it undetectable. Only the full-length protein would carry both domains and thus be detected in our assays. There was no significant difference in the accumulation rate between YFP-luciferase-FKBP and YFP-FKBP-luciferase (P = 0.85, 229 ± 100 s versus 197 ± 83 s) or between YFP–β-Gal–FKBP and YFP-FKBP–β-Gal (P = 0.65, 813 ± 171 s versus 997 ± 334 s) (**Fig. 2a**), strongly suggesting that the observed accumulation rates reflect those of full-length proteins. **Table 1** summarizes the accumulation rates together with other size-related parameters. We also investigated whether the chemical dimerizers themselves could affect primary cilia function. The addition of rapamycin or GA_3-AM alone did not affect cilia length after 1 h (**Supplementary Fig. 10**). This result indicates that nonspecific effects on cilia due to the addition of chemical dimerizers are unlikely to occur over the timescale of our diffusion assays, which were typically complete within 30 min.

The plasma membrane does not exhibit a diffusion barrier

The Stokes-Einstein diffusion equation predicts a linear relationship between diffusion coefficients and the inverse of the Stokes radii (R_s^{-1}) for freely diffusing molecules without any barrier. This was exactly what was observed when rapamycin was used to trap YFP-FKBP fusion proteins at the plasma membrane where a membrane-anchored FRB was expressed (**Fig. 2a** and **Supplementary Fig. 11**). The kinetics of plasma membrane recruitment of our diffusion probes is consistent with the previous observation that diffusion of macromolecules in the cytoplasm is unhindered by barriers[18]. The difference in size dependency on accumulation kinetics (linear for recruitment to the plasma membrane but exponential for recruitment to the cilium) strongly supports the existence of a size-dependent barrier at primary cilia.

Localization of diffusion-limiting components in cilia

Our kinetic data supported the notion of hindered diffusion into primary cilia, but it was not apparent whether diffusion into cilia was limited by a putative barrier at the entrance and structures within cilia or both and how these relationships would evolve for different sized constructs. We reasoned that the time-evolved YFP fluorescence profiles of different FKBP constructs within cilia, as shown in **Figure 1d**, could provide clues to the localization of diffusion-limiting components in cilia. We capitalized on a theory derived from crystal diffusion[19], where analysis of boundary concentrations (analogous to FKBP construct concentrations at the base of cilia) in relation to uptake (accumulated FKBP constructs in cilia) could be used to determine whether the surface permeability (a barrier at the base of cilia) or intracrystalline diffusion (intracilia diffusion) was limiting. Using this analysis, we calculated line scan data from three constructs that spanned the spectrum of our tested size range (3.2–7.9 nm) (**Fig. 3a–c**) and derived the corresponding boundary concentration versus relative uptake plots (**Fig. 3d–f**). Details on how these values were determined can be found in the Online Methods. On the basis of the plots, we calculated a factor, W, which estimates the influence of a permeability barrier versus intracilia factors in regulating uptake into cilia[19]. W values close to 0 indicate that entry into primary cilia is rate determining, whereas W values close to 1 indicate that diffusion within cilia is rate determining. Intermediate W values indicate that both factors contribute to

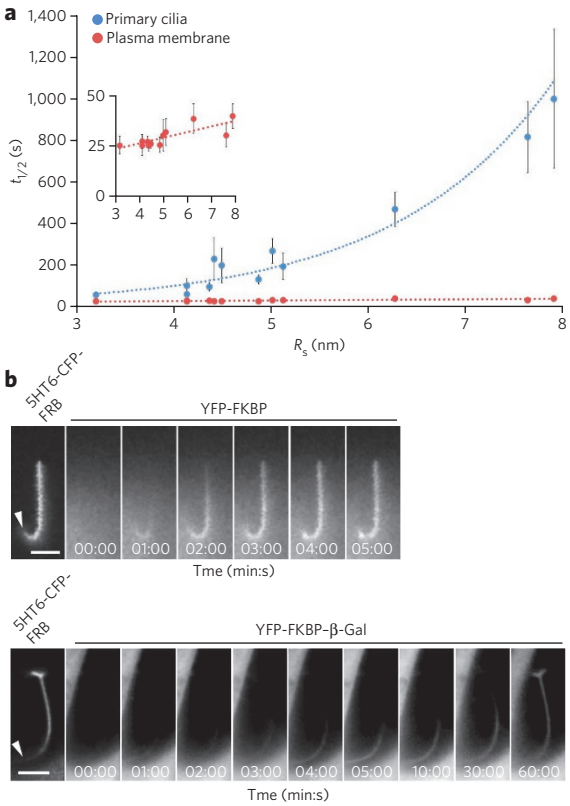

Figure 2 | Exponential dependence of influx rate on size. (**a**) The influx rate of FKBP probe proteins of various sizes into primary cilia. Cells were transfected with 1 of 13 YFP-FKBP probe proteins with either 5HT6-CFP-FRB (primary cilia) or Lyn-CFP-FRB-GAI(S) (plasma membrane). Lyn, plasma membrane–targeting protein. The graph shows the half time ($t_{1/2}$) of influx kinetics of each FKBP probe protein to primary cilia (blue) or plasma membrane (red) as a function of its R_s ($n \geq 10$ cells from three independent experiments). The inset graph indicates a close-up view of the $t_{1/2}$ for plasma membrane trapping. The YFP-FKBP probe proteins tested were as follows (in order of size): YFP-FKBP, YFP-FKBP-PKIM, YFP-FKBP-Grp1(229–772), YFP-FKBP-Grp1(229–1200), YFP-luciferase-FKBP, YFP-FKBP-luciferase, YFP-FKBP-Grp1(1–772), YFP-FKBP-Grp1(1–1200), YFP-FKBP-Tiam1, YFP-FKBP-ΔN β-Gal, YFP-β-Gal-FKBP and YFP-FKBP-β-Gal (PKIM, Grp1, Tiam1, ΔN β-Gal and β-Gal are cytosolic proteins of various sizes). (**b**) Time-series fluorescence images of YFP-FKBP, YFP-FKBP-luciferase and YFP-FKBP-β-Gal inside primary cilia upon addition of 100 nM rapamycin. Images on left indicate 5HT6-CFP-FRB anchored to primary cilia. The arrowheads indicate the base of the cilia. Scale bars, 3 μm.

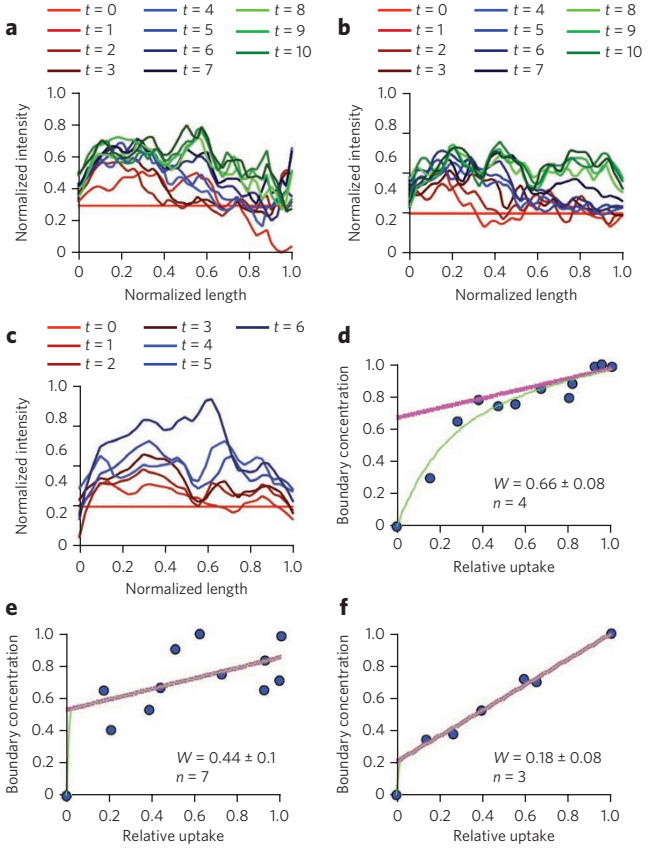

Figure 3 | Localization of ciliary diffusion barriers. (**a**–**c**) Representative examples of YFP fluorescence line scans of indicated constructs through time from the base to tip of cilia. Data are normalized to the line scan at $t = 0$. Constructs shown are YFP-FKBP (**a**), YFP-FKBP-luciferase (**b**) and YFP-β-Gal-FKBP (**c**). (**d**–**f**) Analysis of boundary concentration versus relative uptake of YFP-FKBP (**d**), YFP-FKBP-luciferase (**e**) and YFP-β-Gal-FKBP (**f**). The green line indicates the fit of the following equation: $y = a(1 - e^{cx}) + bx$ (equation (i)). The purple line indicates the fit of $y = a + bx$ (equation (ii)) using coefficients derived from the fit of (i). W denotes the average y-intercept of (ii) from multiple cells along with the s.e.m. The number of cells are indicated.

governing ciliary diffusion. We found a gradation of W values from high to low as FKBP construct size increased (**Fig. 3d–f**), suggesting that as protein size increases, diffusion into cilia is increasingly hindered by a barrier at the base of primary cilia.

A molecular sieve at the base primary cilia

Our analysis suggested that a diffusion barrier at the base of cilia regulates the entry of proteins in a size-dependent manner. To shed light on the physical nature of the barrier, we calculated the diffusion coefficients (D) that characterize the movement of each of the FKBP constructs into primary cilia and then compared them to the D values predicted by various models. We reasoned that the initial flux of FKBP complexes across a proposed diffusion barrier into the cilium could be described by Fick's first law:

$$J = -D\frac{[F_{cy}] - [F_{ci}]}{x} \quad (1)$$

where $[F_{cy}]$ and $[F_{ci}]$ are concentrations of the FKBP construct in the cytoplasm and cilia, respectively; D is the diffusion coefficient of the FKBP construct; and x is the length of the diffusion barrier. We used equation (1) to solve for D for each construct using parameters derived from our experiments ($[F_{cy}]$ and J) and structural details of primary cilia from our experiments and the literature[4,20–23] (**Fig. 4a**). Full details of the measurements and assumptions used can be found in the Online Methods.

As a first step, given that the length of the barrier is unknown, we assessed the effect of varying barrier length on our calculated D values (**Fig. 4b**). We used the Stokes-Einstein equation as an upper boundary for D to confine the range of possible barrier lengths (0–4 μm) (**Fig. 4b**). Our calculated D values showed a linear relationship with barrier length, and for subsequent analysis, we fixed the barrier length at 1.5 μm. Remarkably, the relationship between the experimentally determined D values and the inverse of R_s of the probe proteins was nonlinear, a hallmark of a size-dependent barrier (**Fig. 4c**). This size dependency was independently confirmed by performing FRAP experiments using the smallest and largest probe proteins at primary cilia. The measured diffusion coefficients were 4.3 ± 2.3 μm^2 s^{-1} for GFP-FKBP and 0.3 ± 0.1 μm^2 s^{-1} for GFP-FKBP–β-Gal (**Supplementary Fig. 12**). As the photobleaching was

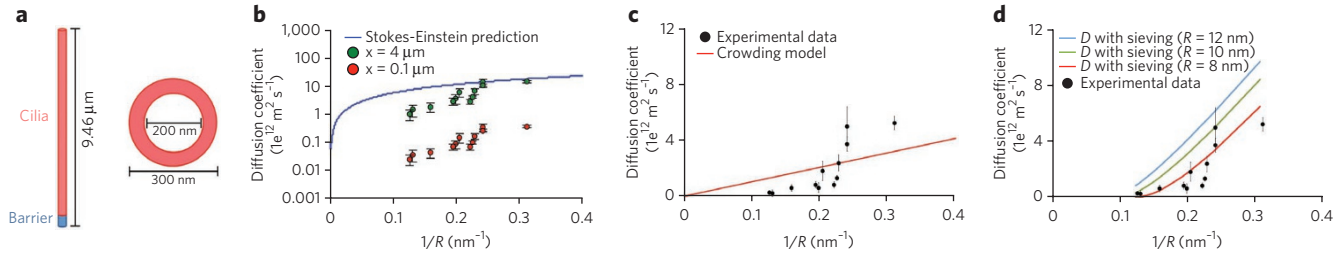

Figure 4 | Analysis of the diffusion barrier at primary cilia. (**a**) Structural depiction of the geometry of the primary cilia used to calculate diffusion coefficients. (**b**) Variation of barrier length and its effect on diffusion coefficients. Increases in the barrier length cause an upward shift in diffusion coefficients. The Stokes-Einstein equation curve is included as an upper boundary to the diffusion coefficients. (**c**) Experimentally derived diffusion coefficients are plotted as a function of the inverse of their R_s in comparison to a molecular crowding model shown in red. (**d**) Experimentally derived diffusion coefficients (D) are plotted as a function of the inverse of their R_s in comparison to a molecular sieving model. The resulting curves for different mesh sizes are included in the plot with an optimal fit at R = 8 nm. The YFP-FKBP probe proteins plotted are as follows (in order of size): YFP-FKBP, YFP-FKBP-PKIM, YFP-FKBP-Grp1(229–772), YFP-FKBP-Grp1(229–1200), YFP-luciferase-FKBP, YFP-FKBP-luciferase, YFP-FKBP-Grp1(1–772), YFP-FKBP-Grp1(1–1200), YFP-FKBP-Tiam1, YFP-FKBP-ΔN β-Gal, YFP–β-Gal–FKBP and YFP-FKBP–β-Gal.

targeted to a ciliary subregion, these values reflect the diffusion both inside and into the primary cilia.

We next assessed the ability of different models of hindered diffusion to account for the discrepancy between predicted and experimentally measured D values. First, we investigated whether molecular crowding in the primary cilia could explain our data by implementing a R_s-independent molecular crowding term[24]

$$\frac{D_c}{D_{sc}} = C \tag{2}$$

where D_c is the D in a molecularly crowded environment, D_{sc} is the D predicted by the Stokes-Einstein equation in cytoplasm, and C is a constant crowding term. We compared D_c values for each FKBP construct to our experimental D values and found that the closest fit, C = 0.19, was a poor fit to our data (R^2 = 0.43, r.m.s. error = 1.31; **Fig. 4c**).

Next, we investigated molecular sieving as a mechanism to explain our observed hindered diffusion. NPCs have been shown to contain a molecular sieve in the lumen, which impedes passive diffusion into the nucleus in a size-dependent manner[25]. We hypothesized that a similar sieve may exist at primary cilia and modeled the sieve with the following equation[25]:

$$\frac{D_m}{D_{sc}} = \left(1 - \frac{r}{R}\right)^2 \tag{3}$$

where D_m is the diffusion coefficient in the mesh, D_{sc} is the diffusion coefficient from the Stokes-Einstein equation in cytoplasm, r is the R_s of the FKBP construct, and R is the estimated mesh radius of the sieve. When we compared D_m for each probe protein with the experimentally derived D values, we found that molecular sieving could indeed provide a reasonable explanation for our data (**Fig. 4d**). The best fit for D_m from our standard cilia geometry (**Fig. 4a**) was obtained with a mean mesh radius of 8 nm (r.m.s. error = 0.90; **Fig. 4d** and **Supplementary Fig. 13a**). One caveat to our analysis is that the calculated mesh radius will vary depending on the assumed barrier length (**Supplementary Fig. 13b**). When we fit the two parameters (mesh radius and barrier length) to our data, the overall best fit was with a mesh radius of 8 nm and a barrier length of 1.4 µm (**Supplementary Fig. 13c**).

DISCUSSION

Chemically inducible dimerization techniques have been used extensively to manipulate the concentration and activity of signaling molecules[12]. In this study, we adapted this technique to probe passive permeability barriers in cells. Specifically, we performed kinetic measurements of the ciliary accumulation of a series of diffusion probes into cilia, and we suggest that the ciliary barrier for soluble proteins consists of a molecular sieve, which hinders the entry of proteins in a size-dependent manner. As more than 90% of the soluble proteins in mammalian cells are smaller than 650 kDa (ref. 26), the size of our largest diffusion probe, our observation implies that most of the cytoplasmic proteins have the potential to freely enter cilia, albeit with kinetics that are determined by protein size. These results have two important implications for our view of how ciliary protein composition is regulated. Over long timescales, the steady-state distribution of proteins in cilia is unlikely to be regulated by a barrier that excludes specific proteins but rather simply by the selective retention of proteins in cilia due to binding interactions with other cilia-resident molecules and by molecular crowding[10]. However, for kinetically controlled, rapid processes, such as signaling reactions, the sieve-like barrier could present an important factor in limiting protein entry, with active or facilitated transport processes playing important regulatory roles.

One of the most well-characterized soluble diffusion barriers in cells are NPCs, which control the passage of biomolecules to and from the nucleus by excluding proteins larger than 60 kDa, slowing down the diffusion of proteins 30–60 kDa in size and allowing anything smaller than 30 kDa to enter[27]. A recent study demonstrated that soluble proteins above a specific size threshold of 67 kDa are restricted from passively entering the primary cilia of epithelial cells in a manner analogous to the NPC[11], in contrast to our result. This study used an end-point assay in which the ciliary distribution of soluble probe proteins was measured 5 min after microinjection into the cytoplasm. Thus, this study could not determine the rates of diffusion of the various test probes, which could easily lead to errors in visualizing the ciliary accumulation of larger, slow-diffusing probes. In contrast, the present chemically inducible diffusion trap at cilia (CIDTc) technique not only provides diffusion kinetics but also bypasses the need for perturbations such as microinjection or detergent permeabilization, preserving the physiological intracellular environment.

Our modeling suggests that the ciliary permeability barrier behaves like a mesh with sieving properties reminiscent of NPCs[25] but with much larger pore radii. The largest pore radius proposed to exist at the NPC is approximately 4.3 nm (ref. 25). However, in our experiments, inert proteins as large as 7.9 nm were able to enter cilia, suggesting that a population of pores larger than 7.9 nm must exist at the cilia base. Our modeling further revealed that a pore radius of 8 nm gave the best fit to our data, but we are unable to rule out the possibility of a heterogeneous distribution of pore radii. The diffusion barrier seen at the base of dendritic spines in neurons[28]

could be more analogous to primary cilia than the nucleus, as neither structure is entirely compartmentalized by lipid membranes. Rather, both compartments are contiguous with the plasma membrane and are decorated by septin molecules at their necks[7,29]. The exponential increases in diffusivity we observed have been similarly noted for large molecules in porous media[30]. This further suggests that porous material at the base of cilia might thus form a molecular sieve, which exponentially affects the entry of proteins into cilia in a size-dependent manner.

Unfixed pores for passive diffusion and preferential retention are both mechanisms observed in the photoreceptor-connecting cilium[10]. Of note, ultrastructural studies on photoreceptor-connecting cilium have not detected any structural features that deviate from primary cilia[4], with some exceptions, such as the specialized cilia of chondrocytes[31]. In connecting cilium photoreceptors, steric volume exclusion is one primary driving force that limits protein accumulation in the outer segment. However, our kinetic analysis revealed that the molecular flux across the cilia barrier rapidly decreased with protein size in the presence of comparable concentration gradients. We suggest that volume exclusion may not be a major defining feature of the ciliary barrier in fibroblasts.

The molecular identity of the sieve-like barrier at the primary cilia is uncertain. Ultrastructural studies have yet to find evidence for such meshwork-like structure at the base of primary cilia. However, these studies have revealed an electron-dense region around the ciliary subcompartment known as the transition zone. Indeed, the transition zone is known to accumulate a series of proteins including nephrocystin complexes (NPHP1, NPHP4 and so on), BBSomes, nucleoporins, Cep290 and Cep164 (refs. 11,32–37). Septin2, a barrier molecule for membrane receptors, also accumulates at the transition zone, which suggests that the transition zone may serve as a molecular sieve for soluble proteins. As nucleoporins form hydrophobic hydrogels at NPCs, they are reasonable candidates for the ciliary barrier[11]. However, given that much larger proteins can passively enter primary cilia, we suggest that the organization of the nucleoporin FG (PheGly)-repeats may be different between these two compartments.

We have used the CIDTc technique to answer fundamental questions about soluble protein diffusion into primary cilia. This method should be useful in future studies aimed at defining the molecular composition of this passive barrier. In principle, this technique should allow the time-resolved, inducible recruitment of any two proteins to primary cilia using the orthogonal recruitment modules we have developed. We believe that this methodology will allow perturbation of ciliary signaling reactions in ways that have previously been impossible, for instance, by the recruitment of signaling proteins such as small GTPases or enzymes that can modulate the amount of second messengers, such as phosphoinositide lipids.

Received 11 March 2013; accepted 5 April 2013;
published online 12 May 2013

METHODS

Methods and any associated references are available in the online version of the paper.

References

1. Singla, V. & Reiter, J.F. The primary cilium as the cell's antenna: signaling at a sensory organelle. *Science* **313**, 629–633 (2006).
2. Veland, I.R., Awan, A., Pedersen, L.B., Yoder, B.K. & Christensen, S.T. Primary cilia and signaling pathways in mammalian development, health and disease. *Nephron Physiol.* **111**, 39–53 (2009).
3. Satir, P. & Christensen, S.T. Overview of structure and function of mammalian cilia. *Annu. Rev. Physiol.* **69**, 377–400 (2007).
4. Nachury, M.V., Seeley, E.S. & Jin, H. Trafficking to the ciliary membrane: how to get across the periciliary diffusion barrier? *Annu. Rev. Cell Dev. Biol.* **26**, 59–87 (2010).
5. Chih, B. *et al.* A ciliopathy complex at the transition zone protects the cilia as a privileged membrane domain. *Nat. Cell Biol.* **14**, 61–72 (2012).
6. Francis, S.S., Sfakianos, J., Lo, B. & Mellman, I. A hierarchy of signals regulates entry of membrane proteins into the ciliary membrane domain in epithelial cells. *J. Cell Biol.* **193**, 219–233 (2011).
7. Hu, Q. *et al.* A septin diffusion barrier at the base of the primary cilium maintains ciliary membrane protein distribution. *Science* **329**, 436–439 (2010).
8. Calvert, P.D., Strissel, K.J., Schiesser, W.E., Pugh, E.N. Jr. & Arshavsky, V.Y. Light-driven translocation of signaling proteins in vertebrate photoreceptors. *Trends Cell Biol.* **16**, 560–568 (2006).
9. Nair, K.S. *et al.* Light-dependent redistribution of arrestin in vertebrate rods is an energy-independent process governed by protein-protein interactions. *Neuron* **46**, 555–567 (2005).
10. Najafi, M., Maza, N.A. & Calvert, P.D. Steric volume exclusion sets soluble protein concentrations in photoreceptor sensory cilia. *Proc. Natl. Acad. Sci. USA* **109**, 203–208 (2012).
11. Kee, H.L. *et al.* A size-exclusion permeability barrier and nucleoporins characterize a ciliary pore complex that regulates transport into cilia. *Nat. Cell Biol.* **14**, 431–437 (2012).
12. DeRose, R., Miyamoto, T. & Inoue, T. Manipulating signaling at will: chemically-inducible dimerization (CID) techniques resolve problems in cell biology. *Pflugers Arch.* **465**, 409–417 (2013).
13. Berbari, N.F., Johnson, A.D., Lewis, J.S., Askwith, C.C. & Mykytyn, K. Identification of ciliary localization sequences within the third intracellular loop of G protein–coupled receptors. *Mol. Biol. Cell* **19**, 1540–1547 (2008).
14. Komatsu, T. *et al.* Organelle-specific, rapid induction of molecular activities and membrane tethering. *Nat. Methods* **7**, 206–208 (2010).
15. Miyamoto, T. *et al.* Rapid and orthogonal logic gating with a gibberellin-induced dimerization system. *Nat. Chem. Biol.* **8**, 465–470 (2012).
16. Celada, F. & Zabin, I. A dimer-dimer binding region in β-galactosidase. *Biochemistry* **18**, 404–406 (1979).
17. Matthews, B.W. The structure of *E. coli* β-galactosidase. *C. R. Biol.* **328**, 549–556 (2005).
18. Seksek, O., Biwersi, J. & Verkman, A.S. Translational diffusion of macromolecule-sized solutes in cytoplasm and nucleus. *J. Cell Biol.* **138**, 131–142 (1997).
19. Kärger, J., Chmelik, C., Heinke, L. & Valiullin, R. A new view of diffusion in nanoporous materials. *Chemie Ingenieur Technik* **82**, 779–804 (2010).
20. Czlapinski, J.L. *et al.* Conditional glycosylation in eukaryotic cells using a biocompatible chemical inducer of dimerization. *J. Am. Chem. Soc.* **130**, 13186–13187 (2008).
21. Narita, K., Kawate, T., Kakinuma, N. & Takeda, S. Multiple primary cilia modulate the fluid transcytosis in choroid plexus epithelium. *Traffic* **11**, 287–301 (2010).
22. Okada, Y., Takeda, S., Tanaka, Y., Izpisua Belmonte, J.C. & Hirokawa, N. Mechanism of nodal flow: a conserved symmetry breaking event in left-right axis determination. *Cell* **121**, 633–644 (2005).
23. Yoshimura, K., Kawate, T. & Takeda, S. Signaling through the primary cilium affects glial cell survival under a stressed environment. *Glia* **59**, 333–344 (2011).
24. Dauty, E. & Verkman, A.S. Molecular crowding reduces to a similar extent the diffusion of small solutes and macromolecules: measurement by fluorescence correlation spectroscopy. *J. Mol. Recognit.* **17**, 441–447 (2004).
25. Mohr, D., Frey, S., Fischer, T., Guttler, T. & Gorlich, D. Characterisation of the passive permeability barrier of nuclear pore complexes. *EMBO J.* **28**, 2541–2553 (2009).
26. Chen, E.I., Hewel, J., Felding-Habermann, B. & Yates, J.R. 3rd. Large scale protein profiling by combination of protein fractionation and multidimensional protein identification technology (MudPIT). *Mol. Cell Proteomics* **5**, 53–56 (2006).
27. D'Angelo, M.A. & Hetzer, M.W. Structure, dynamics and function of nuclear pore complexes. *Trends Cell Biol.* **18**, 456–466 (2008).
28. Nimchinsky, E.A., Sabatini, B.L. & Svoboda, K. Structure and function of dendritic spines. *Annu. Rev. Physiol.* **64**, 313–353 (2002).
29. Tada, T. *et al.* Role of Septin cytoskeleton in spine morphogenesis and dendrite development in neurons. *Curr. Biol.* **17**, 1752–1758 (2007).
30. Sahimi, M. & Jue, V.L. Diffusion of large molecules in porous media. *Phys. Rev. Lett.* **62**, 629–632 (1989).
31. Jensen, C.G. *et al.* Ultrastructural, tomographic and confocal imaging of the chondrocyte primary cilium in situ. *Cell Biol. Int.* **28**, 101–110 (2004).
32. Graser, S. *et al.* Cep164, a novel centriole appendage protein required for primary cilium formation. *J. Cell Biol.* **179**, 321–330 (2007).
33. Hildebrandt, F. & Zhou, W. Nephronophthisis-associated ciliopathies. *J. Am. Soc. Nephrol.* **18**, 1855–1871 (2007).
34. Nachury, M.V. *et al.* A core complex of BBS proteins cooperates with the GTPase Rab8 to promote ciliary membrane biogenesis. *Cell* **129**, 1201–1213 (2007).
35. Salomon, R., Saunier, S. & Niaudet, P. Nephronophthisis. *Pediatr. Nephrol.* **24**, 2333–2344 (2009).

36. Szymanska, K. & Johnson, C.A. The transition zone: an essential functional compartment of cilia. *Cilia.* **1**, 10 (2012).
37. von Schnakenburg, C., Fliegauf, M. & Omran, H. Nephrocystin and ciliary defects not only in the kidney? *Pediatr. Nephrol.* **22**, 765–769 (2007).

Acknowledgments

We thank A. Seki (Stanford University) for the 5HT6 construct, S. Takeda (University of Yamanashi) for the GFP-IFT88 construct and M. Wolfgang (Johns Hopkins University) for β-Gal and luciferase constructs. We also thank D.N.R., T.K., H.I. and S.T. for helpful discussions. This study was supported in part by the US National Institutes of Health (the Baltimore Polycystic Kidney Disease Research and Clinical Core Center provided pilot funds GM092930 and P30 DK090868 to Takanari Inoue and R00CA129174 and R21NS074091 to R.R.) and other grants (Grant-in-Aid for Challenging Exploratory Research 23650197 to H.N. and Pew Foundation to R.R.).

Author contributions

Y.-C.L., S.C.P. and Takanari Inoue generated DNA constructs, and Y.-C.L., S.C.P. and J.J. performed cell biology experiments. B.L. analyzed data with R.R., P.N., A.L. and Takanari Inoue, and P.N. performed biochemical experiments with R.R. H.N. performed FRAP experiments with Takafumi Inoue, Y.-C.L., B.L. and R.R., and Takanari Inoue wrote the paper.

Competing financial interests

The authors declare no competing financial interests.

Additional information

Supplementary information is available in the online version of the paper. Reprints and permissions information is available online at http://www.nature.com/reprints/index.html. Correspondence and requests for materials should be addressed to Takanari Inoue.

ONLINE METHODS

Cell culture and transfection. NIH3T3, IMCD3 cells and HEK 293T cells were maintained at 37 °C in 5% CO_2 in DMEM (Dulbecco's modified Eagle's medium; Gibco) containing 10% FBS (FBS). To induce cilia formation, cells were cultured for 24 h in a 0.2% serum containing cell culture medium. DNA plasmid transfection was performed with FuGENE HD (Roche) 24 h before the serum starvation.

DNA constructs. The constructs, YFP-FKBP and YFP-FKBP-Tiam1(C580), have been previously reported[38]. For the constructs YFP-FKBP-PKIM, YFP-FKBP-luciferase, YFP-FKBP–β-Gal(ΔN) and YFP-FKBP–β-Gal, we performed a polymerase chain reaction (PCR) that flanks a target nucleotide with EcoRI and BamHI. The PCR products were subsequently inserted into the multi cloning site of the YFP-FKBP plasmid. For the constructs YFP-FKBP-Grp1(229–772), YFP-FKBP-Grp1(229–1200), YFP-FKBP-Grp1(1–772) and YFP-FKBP-Grp1(1–1200), we performed a similar PCR that flanks a target nucleotide with XhoI and KpnI, which were again inserted into the multicloning site of the YFP-FKBP plasmid. For the construct YFP-luciferase-FKBP and YFP–β-Gal–FKBP, we first constructed YFP-PSD95-FKBP by performing a similar PCR that flanks a PSD95 with EcoRI and KpnI, which were inserted into the multicloning site of the YFP plasmid. We then excised YFP-PSD95 using NheI and KpnI, which was inserted into the engineered FKBP plasmid that has the multicloning sites both at the N and C termini[14]. YFP-luciferase-FKBP and YFP–β-Gal–FKBP were constructed by replacing the PSD95 of the YFP-PSD95-FKBP construct with a PCR product encoding luciferase or β-Gal using EcoRI and Asp718I or BsrGI and Asp718I, respectively. 5HT6-CFP-FRB was constructed by first mutating the NheI site of 5HT6 and then conducting PCR that includes 5HT6 flanked with NheI and AgeI restriction sites. The resulting PCR product was ligated with CFP-FRB plasmid already digested with NheI and AgeI. The correct nucleotide sequences of each construct were confirmed.

Gel filtration. Each of the constructs was transfected using calcium phosphate into a plate of HEK293T cells. The cells were harvested in (phosphate buffered saline (PBS) 48 h after transfection, and cytosolic protein was extracted by hypotonic lysis. Briefly, the cells were spun down, PBS was removed, and the cells were resuspended in hypotonic lysis buffer (20 mM HEPES, pH 7.4, 5 mM KCl, 1 mM DTT, 1× SigmaFAST). The cells were incubated and swollen on ice for 30 min and then snap-frozen and quick thawed twice. The cells were sheared with a needle, and nuclei were spun out at 2,500*g* for 5 min. The salt was adjusted to 300 mM KCl. The cytosolic supernatant was centrifuged at 100,000*g* for 30 min, and the resulting supernatant was filtered through a 0.2-μm filter. The final protein concentration was approximately 4–5 mg/mL. The extract (100 μL) was loaded onto a Superdex 200 10/300 GL gel filtration column equilibrated in buffer containing 20 mM HEPES, pH 7.4, 300 mM KCl and 1 mM DTT. The protein was eluted isocratically with the same buffer at 0.25 mL/min, and 0.25-mL fractions were collected. The YFP fluorescence of each fraction was measured in a Bio-Tek Synergy H1 hybrid plate reader (excitation: 488 nm, emission: 530 nm), and the results were plotted and aligned with the absorbance plots from the chromatograms. V_e for each protein was calculated based on the fraction containing the peak fluorescence value, and the R_s was calculated by interpolating from known R_s values of standards used to calibrate the column. The formula used for interpolation was from ref. 39: $(-\log(K_{av}))^{1/2} = a + R_s \times b$, where $K_{av} = (V_e - V_0)/(V_t - V_0)$.

Live-cell imaging. Cells were transfected with indicated constructs, incubated for 24 h, and then serum starved for 18–24 h before imaging. Live-cell imaging was performed with a 63× oil objective (ZEISS) mounted on an inverted Axiovert135TV microscope (ZEISS) equipped with a motorized stage (ASI). Fluorescence images were collected by a QIClick charge-coupled device camera (QImaging) every 30 s for 10 min to 1 h, except for the experiments shown in **Figure 1**, where images were taken every 10 s over 20 min.

FRAP experiments. Fluorescence images of 5HT6-GFP, 5HT6-GFP-FRB and GFP-IFT88 were collected using a FV-1000 confocal system (OLYMPUS) equipped with 60× NA 1.45 oil immersion lens. The confocal aperture was set to be the maximum to compensate for possible movement of the cilia and the drift of the focal plane. In long-term (90-min) experiments, photobleaching was carried out with a 473-nm laser of 10% intensity relative to that used in short-term (10 min) experiments, so that the proper focal plane could be tracked by the imaging with minimal intensity of excitation light before each frame. To quantify the diffusion coefficient of fluorescent fusion proteins in primary cilia, a fraction of cilia containing the tip was scanned with intense 473-nm laser irradiation for 100 ms for photobleaching. Relaxation of the resultant fluorescence intensity gradient was analyzed as previously described[40], with a minor modification; both spatial and temporal grids or steps used for the model computation were set by dividing the actual pixel size and frame interval by integer factors, which were gradually increased until the deviations of the fitting converge.

Analysis of boundary concentrations and relative uptake. Boundary concentrations were determined by taking the maximum fluorescence intensity of each line scan within the first 25% of the length of cilia to account for fluctuations arising from noise. Relative uptake was determined by integrating each line scan and normalizing to the maximal uptake. Boundary concentration versus relative uptake plots were fitted by the following equation:

$$y = a(1 - e^{cx}) + bx \tag{4}$$

using the 'fit' command in Matlab. As the relative uptake approaches saturation, the curve becomes linear[19] and can be approximated by a line defined by:

$$y = a + bx \tag{5}$$

with coefficients defined by the previous fit in (4). The *W* values denoted in **Figure 3d–f** were taken as the *y*-intercept (*a*) from (5).

Initial slope analysis. We applied a linear fit to the first four time points of the influx curves (example shown in **Fig. 1e**) of each FKBP construct and obtained a mean slope for each.

Calculation of diffusion coefficients into primary cilia. *Assumptions.* The first assumption we make is that at early time points after rapamycin addition, the initial concentration of free diffusing FKBP complexes in the primary cilia is zero ($[F_{ci}] = 0$) after rapid trapping to FRB constructs. On the basis of this assumption, we can rewrite (1) as:

$$J = -D\frac{[F_{cy}]}{x} \tag{6}$$

The flux, *J*, can be restated as the number of molecules that pass through the diffusion barrier into the cilium in a given time through a cross-sectional area.

$$J = -\frac{1}{A}\frac{dNF_{ci}}{dt} \tag{7}$$

Here *A* is the cross sectional area of the cilia barrier, and NF_{ci} is the total number of molecules of the FKBP construct (free and FRB-bound) in the cilium. We can combine equation (6) and equation (7) to solve for *D*.

$$D = \frac{dNF_{ci}}{dt}\frac{x}{[F_{cy}]A} \tag{8}$$

Calculations. To calculate *D* for each YFP-tagged FKBP construct, we first calculated $\frac{dNF_{ci}}{dt}$ by taking the slope of the integrated intensity of YFP over the first 90 s in the cilia. Next, to measure $[F_{cy}]$, we measured the integrated intensity of YFP in three defined regions in the cytoplasm and took their average as the number of molecules in the cytoplasm. We divided this value by the unit volume in this region to obtain $[F_{cy}]$. Our estimates for the volume were based on the area of the region of analysis and an estimated cellular height of 6 μm. Finally, we calculated *A* on the basis of our assumed cilia geometry (**Supplementary Fig. 13a**). The barrier length, *x*, was an unknown in (6) and thus was varied to assess its affect on *D* (**Supplementary Fig. 13b**).

Geometry. We used the average cilia length from our data (**Supplementary Fig. 8**) and the structural details obtained from previous works[4,20–23] for the

doi:10.1038/nchembio.1252

cross-sectional area, *A*. We simplified the primary cilia into two concentric cylinders with radii of 200 nm and 300 nm, respectively, and an overall cilia length of 9.46 μm (**Supplementary Fig. 11a**). The smaller cylinder functions as a proxy for the axoneme, the nine microtubule doublets defining the structure of the primary cilia, and no diffusion of soluble proteins is assumed to occur in the inner lumen. The outer rod is representative of the plasma membrane enclosing the primary cilia.

38. Inoue, T., Heo, W.D., Grimley, J.S., Wandless, T.J. & Meyer, T. An inducible translocation strategy to rapidly activate and inhibit small GTPase signaling pathways. *Nat. Methods* **2**, 415–418 (2005).
39. Laurent, T.C. & Killander, J. A theory of gel filtration and its experimental verification. *J. Chromatogr. A* **14**, 317–330 (1964).
40. Fukatsu, K. *et al.* Lateral diffusion of inositol 1,4,5-trisphosphate receptor type 1 is regulated by actin filaments and 4.1N in neuronal dendrites. *J. Biol. Chem.* **279**, 48976–48982 (2004).